

# On the velocity dispersion of young star clusters: super-virial or binaries?

M. Gieles<sup>1\*</sup>, H. Sana<sup>1,2</sup> and S. F. Portegies Zwart<sup>3</sup>

<sup>1</sup> *European Southern Observatory, Casilla 19001, Santiago 19, Chile*

<sup>2</sup> *Astronomical Institute ‘Anton Pannekoek’, University of Amsterdam, Kruislaan 403, 1098 SJ Amsterdam, the Netherlands*

<sup>3</sup> *Leiden Observatory, Leiden University, PO Box 9513, 2300 RA Leiden, the Netherlands*

Accepted 2009 November 5. Received 2009 October 26; in original form 2009 September 23

## ABSTRACT

Many young extra-galactic clusters have a measured velocity dispersion that is too high for the mass derived from their age and total luminosity, which has led to the suggestion that they are not in virial equilibrium. Most of these clusters are confined to a narrow age range centred around 10 Myr because of observational constraints. At this age the cluster light is dominated by luminous evolved stars, such as red supergiants, with initial masses of  $\sim 13\text{--}22 M_{\odot}$  for which (primordial) binarity is high. In this study we investigate to what extent the observed excess velocity dispersion is the result of the orbital motions of binaries. We demonstrate that estimates for the dynamical mass of young star clusters, derived from the observed velocity dispersion, exceed the photometric mass by up-to a factor of 10 and are consistent with a constant offset in the square of the velocity dispersion. This can be reproduced by models of virialised star clusters hosting a massive star population of which  $\sim 25\%$  is in binaries, with typical mass ratios of  $\sim 0.6$  and periods of  $\sim 1000$  days. We conclude that binaries play a pivotal role in deriving the dynamical masses of young ( $\sim 10$  Myr) moderately massive and compact ( $\lesssim 10^5 M_{\odot}$ ;  $\gtrsim 1$  pc) star clusters.

**Key words:** globular clusters: general – open clusters and associations: general – galaxies: star clusters – binaries: general – binaries: spectroscopic – supergiants

## 1 INTRODUCTION

Young massive clusters have received considerable attention in the last decade because they trace star formation (e.g. Whitmore & Schweizer 1995; Miller et al. 1997; Zepf et al. 1999). Advances in observations enabled us to resolve such star clusters up to  $\sim 20$  Mpc, allowing determination of their fundamental parameters, such as mass and radius (e.g. Larsen 2004).

The mass of a resolved star cluster can be determined in two ways: one of them by converting the observed luminosity, age and distance directly to mass via the age dependent mass-to-light ratio ( $M/L$ ) taken from a single stellar population (SSP) model. We refer to the resulting mass as the photometric mass  $M_{\text{phot}}$ . This method requires an estimate of the cluster age, which again requires estimates for the metallicity and the stellar initial mass function (IMF).

An independent mass estimate is based on the virial theorem and this mass is generally referred to as the dynamical mass (Spitzer 1987):

$$M_{\text{dyn}} = \frac{\eta \sigma_{\text{dyn}}^2 r_{\text{eff}}}{G}. \quad (1)$$

Here  $G$  is the gravitational constant,  $\sigma_{\text{dyn}}$  is the line of sight velocity

dispersion in the cluster,  $r_{\text{eff}}$  is the effective (half-light) radius<sup>1</sup> and  $\eta \simeq 9.75$  is a constant that depends slightly on the density profile.

Equation (1) is valid for a cluster in virial equilibrium consisting of single stars. Since in this study we consider possible difference between  $\sigma_{\text{dyn}}$  and the observed velocity dispersion,  $\sigma_{\text{obs}}$ , we will refer to the empirically derived dynamical mass, i.e. based on  $\sigma_{\text{obs}}$ , as  $M_{\text{dyn}}^{\text{obs}}$ .

A comparison between  $M_{\text{phot}}$  and  $M_{\text{dyn}}^{\text{obs}}$  serves as a check for the range of assumptions on which both mass estimates are based. An inconsistency between  $M_{\text{phot}}$  and  $M_{\text{dyn}}^{\text{obs}}$  can be attributed to variations in the IMF, on which  $M_{\text{phot}}$  is in part based, or to a lack of virial equilibrium, on which  $M_{\text{dyn}}^{\text{obs}}$  is based. For many young ( $\sim 10$  Myr) star clusters  $M_{\text{dyn}}^{\text{obs}} > M_{\text{phot}}$ , with  $M_{\text{dyn}}^{\text{obs}}$  up to  $\sim 10$  times larger than  $M_{\text{phot}}$  (e.g. Bastian et al. 2006, hereafter B06), suggesting that these objects are super-virial. For older clusters ( $\gtrsim 100$  Myr) there is good agreement between  $M_{\text{dyn}}^{\text{obs}}$  and  $M_{\text{phot}}$  (e.g. Larsen et al. 2004, B06).

The alleged super-virial state of some young clusters has been attributed to the impulsive expulsion of residual gas from

<sup>1</sup> Here we assume that the half-light radius is the same as the half-mass radius, which is not the case when the cluster is mass segregated (Fleck et al. 2006; Gaburov & Gieles 2008).

the parent molecular cloud in which the star cluster formed (e.g. Goodwin & Bastian 2006). Such early outgassing, driven by stellar winds of massive stars or supernovae, causes the stellar velocities to be high compared to the binding energy of the stars. This argument has been used to motivate infant mortality of young star clusters (Lada & Lada 2003).

However, the gas expulsion theory has difficulties in explaining the super-virial velocity for the 10 Myr old clusters presented in B06. The arguments are as follows: The time needed to completely dissolve, or to find a new virial equilibrium after impulsive gas expulsion is about 20 crossing times,  $t_{\text{cr}}$ , where  $t_{\text{cr}} \propto \rho_{\text{h}}^{-1/2}$  and  $\rho_{\text{h}}$  is the density within the half-mass radius (see for example Fig. 8 in Baumgardt & Kroupa 2007). Hence, to be able to ‘catch’ an unbound or expanding cluster at 10 Myr,  $t_{\text{cr}}$  should be  $\gtrsim 1$  Myr. This corresponds to a half-mass density of stars and gas of  $\rho_{\text{h}} \lesssim 300 M_{\odot} \text{pc}^{-3}$ . Clusters with shorter  $t_{\text{cr}}$  (higher density) have expanded into the field, or found a new equilibrium, a few Myrs after gas expulsion and are not observable as super-virial clusters at 10 Myr<sup>2</sup>. The density in the embedded phase of the clusters under discussion is unknown, but can be roughly estimated using their current densities. The present day densities are  $\rho_{\text{h}} \approx 10^{3 \pm 1} M_{\odot} \text{pc}^{-3}$  (Table 3). The densities in the embedded phase were at least a factor  $1/\epsilon^4$  higher, where  $\epsilon$  is the star formation efficiency. This because the mass of the embedded cluster has reduced by a factor  $\epsilon$  and the cluster has expanded at least by a factor of  $1/\epsilon$  as a response to it, contributing a factor  $1/\epsilon^3$  to the reduction of  $\rho_{\text{h}}$ . The  $1/\epsilon$  expansion holds for adiabatic mass loss, for impulsive mass loss and  $\epsilon \lesssim 0.9$  the cluster expands much more (Hills 1980). So for the clusters at 10 Myr the estimated densities in the embedded phase are much too high to still have features of gas expulsion detectable in their velocity dispersion at 10 Myr. These arguments suggest that deviations from virial equilibrium are not a plausible explanation and an alternative explanation for the high  $\sigma_{\text{obs}}$  values is needed.

The existence of binary stars is generally ignored in the estimates for  $M_{\text{dyn}}^{\text{obs}}$ , even though their internal velocities can lead to an over estimation of  $M_{\text{dyn}}$  (Kouwenhoven & de Grijs 2008, hereafter K08). K08 studied this phenomenon in virialised star clusters with a 100% binary fraction and a range of  $\sigma_{\text{dyn}}$ . They subsequently derive  $M_{\text{dyn}}^{\text{obs}}$  by ‘measuring’  $\sigma_{\text{obs}}$  and applying equation (1). They found that the presence of binaries can lead to an overestimation of  $M_{\text{dyn}}$  by a factor of  $\sim 2$  for clusters with  $\sigma_{\text{dyn}} \simeq 1 \text{ km s}^{-1}$ . For clusters with  $\sigma_{\text{dyn}} \simeq 10 \text{ km s}^{-1}$  they found only a 5% increase in  $M_{\text{dyn}}^{\text{obs}}$  due to binaries. They therefore concluded that binaries are not important for massive/dense clusters. Mengel et al. (2008, hereafter M08) found  $M_{\text{dyn}}^{\text{obs}}/M_{\text{phot}} \simeq 10$  for some of the star clusters in the Antennae galaxies (NGC 4038/4039) and NGC 1487 and since these clusters have velocity dispersions of  $10 - 20 \text{ km s}^{-1}$  they subsequently concluded that binaries are not important and that these star clusters are super-virial and dissolving quickly.

Here we revisit the effect of binaries on  $M_{\text{dyn}}^{\text{obs}}/M_{\text{phot}}$  and we focus on  $\sim 10$  Myr old star clusters. This is motivated by our desire to incorporate the effect of the steep increase of the stellar luminosity with increasing stellar mass, which is in particular important for young clusters, an aspect not considered by K08. Of the two approaches presented by K08, one focused on solar-type stars, the other uses a Kroupa IMF for the primary stars. They give equal

weight to each binary in their computed velocity dispersion. In addition K08 do not consider stars more massive than  $20 M_{\odot}$ . This approach may be appropriate for studies of intermediate age and old open star clusters, but it is less suitable for young star clusters.

At an age of  $\sim 10$  Myr the cluster light is dominated by the most massive ( $\gtrsim 15 M_{\odot}$ ) stars for which binarity is high and ignoring them can lead to misinterpretations of observations of various astrophysical processes (e.g. Vanbeveren et al. 1998). Massive binaries have a larger effect on  $\sigma_{\text{obs}}$  than low-mass binaries due to their higher orbital velocities, but also due to the more common short-periods and comparable masses (e.g. Duquennoy & Mayor 1991; Portegies Zwart et al. 2002; Sana et al. 2008, 2009; Mason et al. 2009). Incorporating the massive stars in our calculation has two important effects, both of which amplify the effect of binarity on  $\sigma_{\text{obs}}$  with respect to the results of K08: massive stars dominate the cluster light and their higher masses and (intrinsically) different binary properties give rise to a larger  $\sigma_{\text{obs}}$ .

In this paper we quantify the effect of the presence of (massive) binaries on  $M_{\text{dyn}}^{\text{obs}}/M_{\text{phot}}$  and we use this ratio as a proxy of the excess dispersion. In Section 2 we discuss the properties of the binary population that is expected in young ( $\sim 10$  Myr) clusters and we present a simple model for the additional velocity dispersion due to such binaries. In Section 3 we summarize existing observational results to confront our model with. Our conclusions are discussed in Section 4. All the specific acronyms used in this study and their definitions are given in Table 1.

## 2 THE VELOCITY DISPERSION DUE TO BINARITY

### 2.1 The importance of massive binaries

The young clusters with measured  $M_{\text{dyn}}^{\text{obs}}$  and  $M_{\text{phot}}$  have a rather narrow range in ages of  $\sim 8 - 13$  Myr. This is mainly because of the onset of red supergiants in this age range making clusters brighter and easier to detect and study in detail. Stars in a stellar population with an age of 10 Myr have initial mass of  $13 - 22 M_{\odot}$ , corresponding to masses of  $13 - 16 M_{\odot}$  at an age of 10 Myr (Lejeune & Schaerer 2001). If we would consider a small spread around 10 Myr the quoted mass range would be slightly larger, but for simplicity will continue with the assumption of a constant age of 10 Myr. Those massive stars appear to have high primordial multiplicity with a spectroscopic binary fraction of  $\sim 50\%$  or more (i.e.  $f \gtrsim 0.5$ , Mason et al. 2009; Bosch et al. 2009).

Most of the measurements we discuss in Section 3 are done in the near infrared. At these wavelengths red supergiants (RSGs) dominate the observed light and therewith the measured  $\sigma_{\text{obs}}$ . For the studies done in the optical wavelength the blue supergiants (BSGs) are more dominant. We here refer to the population of luminous evolved stars as supergiants (SGs) and use the subscripts SG to denote parameters that apply to these stars.

Since the SGs outshine the main sequence stars it is important to establish the binary fraction among them. This estimate is complicated by the internal evolution of binary stars affecting especially the RSG phase and hence the actual population of SGs present at an age of 10 Myr. In particular, short-period binaries are likely to experience a common envelope evolution (CEE) and/or Roche-lobe overflow (RLOF) which causes the binary components to follow a different evolution compared to single stars of similar initial mass, and may prevent the RSG stage altogether.

Eldridge et al. (2008, hereafter E08) find that these effects reduce the average duration of the RSG phase by a factor of two or

<sup>2</sup> The models of Goodwin & Bastian (2006) start with a density of  $\sim 60 M_{\odot} \text{pc}^{-3}$  ( $t_{\text{cr}} \approx 2.5$  Myr) in the embedded phase, and this is why they find that the effects of gas expulsion are observable for 25 Myr.

three. They find this for a population of binaries with a flat distribution in  $\log P/d$  between  $-0.15$  and  $4.5$  and a flat distribution of  $q$  between  $0.1$  and  $0.9$ , where  $P$  and  $q$  are the orbital period and the ratio of the secondary mass over the primary mass, respectively. The short period binaries with high mass ratios are most affected by interactions through RLOF and CEE. For our simple model we assume a minimum period,  $P_{\text{crit}}$ , and as an approximation of the shortened evolved phase of primaries in tight binaries we remove the binaries with  $P < P_{\text{crit}}$ . The fraction of binaries we remove should roughly match the fractional reduction of the average life-time of the RSGs (factor of  $2 - 3$ ). This constraint is met for  $P_{\text{crit}} = 500$  d since 63% of the binaries in the E08 population have  $P < 500$  d for  $m_1 = 15 M_{\odot}$ .

RSGs at 10 Myr have a maximum radius of  $\sim 900 R_{\odot}$ . For  $m_1 = 15 M_{\odot}$  and  $q = 0.6$  this corresponds roughly to the separation of a binary with  $P_{\text{crit}}$ . For  $P = 2000$  d the Roche-lobe radius is around  $900 R_{\odot}$  (using the formula of Eggleton 1983) and binaries with longer orbital periods will follow an evolutionary path similar to single stars (08). So in our model we remove all binaries with  $P < 500$  d and assume that binaries with  $P > 500$  d experience a SG phase unaffected by binary evolution, even though it is expected that the RSG phase of primaries in binaries with  $500 < P/d < 2000$  is affected by the companion. In reality it will not be such a step function, since most SGs do contribute at some stage in their evolution to the integrated light. But under our assumptions we reduce the number of binaries roughly by the same fraction as what was found for the fractional reduction of the average RSG phase in the model of E08. By removing all binaries with  $P < 500$  d we are probably making a conservative approach since we bias our binary population to longer periods. In reality these binaries can continue to contribute to the velocity dispersion. This because the primary does not necessarily becomes dark after its shortened RSG phase, and if it does, the secondary can still contribute to the velocity dispersion (E08).

The relevant parameter for studying the binaries that contribute to the velocity dispersion is the fraction of binaries among SGs, which we identify with  $f_{\text{SG}}$ . Using  $N_{\text{p}}$  for the number of stars with initial masses in the range  $13 - 22 M_{\odot}$  and the fraction of binaries with an orbital period  $P > P_{\text{crit}}$  as  $g$ , then the number of stars in binaries unaffected by interaction is  $gfN_{\text{p}}$  and the number of SGs that is removed is  $(1 - g)fN_{\text{p}}$ . The total number of remaining SGs, i.e. single and in binaries, is  $(1 - f)N_{\text{p}} + gfN_{\text{p}}$ . So we can write for  $f_{\text{SG}}$

$$f_{\text{SG}} = \frac{gf}{(1 - f) + gf}. \quad (2)$$

In equation (2) we have neglected the possibility that secondary stars contribute to the SG population, thus slightly underestimating  $f_{\text{SG}}$ . If all stars are in binaries ( $f = 1$ ) then  $f_{\text{SG}} = f$  for all values of  $g$ . For the remainder of our analysis we adopt a more conservative value of  $f = 0.6$  in our parametric model (Section 2.2) and a range  $0.3 < f < 0.9$  for the Monte Carlo simulations in Section 2.3.

The orbital periods of early-type spectroscopic binaries range from a couple of days to about 10 years. Adopting an Öpik's law in the interval  $0.3 < \log P/d < 3.5$  and a period threshold  $\log P_{\text{crit}}/d = 2.7$  we find  $g = 0.25$  (i.e. we remove 75% of the binaries), which via equation (2) results in  $f_{\text{SG}} \simeq 0.25$ . For the representative period we use  $P = 10^3$  d, which is approximately the mean of the periods above  $P_{\text{crit}}$  when assuming a flat distribution in  $\log P$ .

The distribution of mass ratios for high-mass stars appears to be flat between  $q \simeq 0.2$  (the typical detection limit for SB2 sys-

**Table 1.** Overview of the specific acronyms used in this study.

Acronym	Description
$f$	primordial binary fraction of massive stars ( $13 - 22 M_{\odot}$ )
$g$	fraction of primordial binaries unaffected by interaction
$f_{\text{SG}}$	effective binary fraction among SGs at 10 Myr
$m_1$	mass of the primary star
$N_{\text{p}}$	number of stars with initial masses in the range $13 - 22 M_{\odot}$
$q$	ratio of the secondary mass over the primary mass
$P$	orbital period
$P_{\text{crit}}$	minimum period for binaries to be unaffected by interaction
$v_{\text{orb}}$	orbital velocity of the primary star
$v_{\text{1D}}$	line of sight velocity of the primary star
$r_{\text{eff}}$	cluster half-light radius in projection
$\sigma_{\text{dyn}}$	1D dynamical velocity dispersion of cluster members
$\sigma_{\text{obs}}$	empirically determined 1D velocity dispersion
$\sigma_{\text{bin}}$	1D velocity dispersion due to binary orbital motions
$M_{\text{dyn}}$	dynamical cluster mass based on $\sigma_{\text{dyn}}^2$
$M_{\text{dyn}}^{\text{obs}}$	empirically determined dynamical mass based on $\sigma_{\text{obs}}^2$
$M_{\text{phot}}$	photometric cluster mass

tems) and  $q = 1$  (e.g. Sana & Le Bouquin 2009). We adopt  $q = 0.6$  as a typical value for the mass ratio.

Our adopted values of the parameters that control the SG binary population at 10 Myr are summarised in Table 2. These values serve as input for the model presented in the next section.

## 2.2 A parametric model for the velocity contribution of binaries

To quantify the importance of binaries on  $\sigma_{\text{obs}}$  we model their observational characteristics. Since the dynamical velocities of the cluster members (stars and centres of mass of binaries) and the orbital velocities of the binary members are uncorrelated, we can write  $\sigma_{\text{obs}}^2 = \sigma_{\text{dyn}}^2 + \sigma_{\text{bin}}^2$ . Here we derive a simple expression for the contribution to  $\sigma_{\text{obs}}^2$  of the orbital motions of binaries,  $\sigma_{\text{bin}}^2$ .

Since the secondary is generally much fainter than the primary we ignore its contribution to the light and focus only on the primary star. Its orbital velocity,  $v_{\text{orb}}$ , can be expressed in terms of  $q$ ,  $m_1$  and  $P$  using Kepler's third law:

$$v_{\text{orb}} = q \left( \frac{2}{1 + q} \right)^{2/3} \left( \frac{\pi G m_1}{2P} \right)^{1/3}. \quad (3)$$

The contribution to the line of sight velocity,  $v_{\text{1D}}$ , depends on the inclination,  $i$ , of the orbital plane and the phase,  $\theta$ , in which the binary is observed. We first assume a population of binaries with the same  $q$ ,  $m_1$  and  $P$  and random orientations of the orbital planes and (un-correlated) random orbital phases. This results in flat distributions of  $-1 \leq \cos(i) \leq +1$  and  $0 \leq \theta \leq 2\pi$ . For each individual binary  $v_{\text{1D}} = v_{\text{orb}} \sin(i) \cos(\theta)$  so the distribution of  $v_{\text{1D}}$  values is the joint probability density function of  $\sin(i)$  and  $\cos(\theta)$  multiplied by  $v_{\text{orb}}$ , which is flat between  $-v_{\text{orb}}$  and  $+v_{\text{orb}}$ . The variance of this distribution is  $\sigma_{\text{bin}}^2 = v_{\text{orb}}^2/3$ . In reality there will be a spread in the binary parameters which will make the line of sight velocity distribution peaked, with a similar variance. We continue with the assumption of a population of identical binaries to be able to analytically express our result in the binary parameters. In Section 2.3 we validate this assumption and quantify the expected spread using Monte Carlo simulations.

Taking into account that only a fraction  $f_{\text{SG}}$  (Section 2.1) of the stars that contribute to the cluster light is part of a binary re-

**Table 2.** Adopted values for the parameters of SG binaries at 10 Myr.

parameter	Reference	Range		
		min	max	distribution
$f$	0.6	0.3	0.9	flat
$g$	0.25	–	–	–
$f_{\text{SG}}$	0.25	–	–	–
$m_1/M_\odot$	15	13	16	Salpeter
$q$	0.6	0.2	1.0	flat
$\log P/\text{d}$	3.0	0.3	3.5	flat
$\log P_{\text{crit}}/\text{d}$	2.7	2.7	2.7	–

duces  $\sigma_{\text{bin}}^2$  by a factor  $f_{\text{SG}}$ . The dependence of  $\sigma_{\text{bin}}^2$  on the binary parameters can then be expressed as

$$\sigma_{\text{bin}}^2 = \left(\frac{f_{\text{SG}}}{3}\right) \left(\frac{2q^{3/2}}{1+q}\right)^{4/3} \left(\frac{\pi G m_1}{2P}\right)^{2/3}. \quad (4)$$

For the reference values (Table 2) we find that  $\sigma_{\text{bin}} \simeq 6.6 \text{ km s}^{-1}$ , which is equal to  $\sigma_{\text{dyn}}$  for a (virialised) cluster with  $M = 10^5 M_\odot$  and  $r_{\text{eff}} = 1 \text{ pc}$  (equation 1). So for such clusters and these binary parameters  $M_{\text{dyn}}^{\text{obs}}$  overestimates the true mass  $M$  by a factor of two because of binaries. We use these scaling values to write a more general expressing for the ratio

$$\frac{\sigma_{\text{bin}}^2}{\sigma_{\text{dyn}}^2} \simeq \left(\frac{f_{\text{SG}}}{0.25}\right) \left(\frac{q}{0.6}\right)^{3/2} \left(\frac{m_1}{15M_\odot}\right)^{2/3} \left(\frac{10^3 \text{d}}{P}\right)^{2/3} \left(\frac{M/r_{\text{eff}}}{10^5 M_\odot \text{pc}^{-1}}\right)^{-1}, \quad (5)$$

where we have approximated the term  $[2q^{3/2}/(1+q)]^{4/3}$  from equation (4) by  $q^{3/2}$ . Equation (5) is accurate to within 8% for  $q \gtrsim 0.2$ .

In the next section we will use the ratio  $M_{\text{dyn}}^{\text{obs}}/M$  as a measure of the excess dispersion, which we can write as

$$\frac{M_{\text{dyn}}^{\text{obs}}}{M} = \frac{\sigma_{\text{dyn}}^2 + \sigma_{\text{bin}}^2}{\sigma_{\text{dyn}}^2}, \quad (6)$$

$$\simeq 1 + \left(\frac{M/r_{\text{eff}}}{10^5 M_\odot \text{pc}^{-1}}\right)^{-1}, \quad (7)$$

where in the last step we have used the reference values of Table 2 such that the binary part of equation (5) equals 1.

For  $M/r_{\text{eff}} < 10^5 M_\odot \text{pc}^{-1}$  binaries dominate the measured velocities and therefore  $M_{\text{dyn}}^{\text{obs}}/M \propto (M/r_{\text{eff}})^{-1}$  (for a constant  $\sigma_{\text{bin}}^2$ ). For higher values of  $M/r_{\text{eff}}$  the presence of binaries has little effect on the estimated mass and  $M_{\text{dyn}}^{\text{obs}}/M \simeq 1$ .

### 2.3 A Monte Carlo validation

Up to this point we have assumed populations of equal binaries giving a flat distribution of  $v_{1\text{D}}$  values and a fixed value for  $\sigma_{\text{bin}}$  for each cluster. First we verify the assumption that the shape of the  $v_{1\text{D}}$  distribution resembles a Gaussian when a range of binary parameters is assumed (Section 2.3.1). Then we quantify the expected spread in  $\sigma_{\text{bin}}^2$  values when comparing clusters (Section 2.3.2).

#### 2.3.1 The velocity dispersion of a binary population

We generate two populations of  $10^4$  binaries, i.e. no single stars, to study the shape of the velocity dispersion of their orbital motions. For one population we give all primaries a  $v_{\text{orb}}$  based on equation (3) and the reference values from Table 2. The values of  $v_{1\text{D}}$

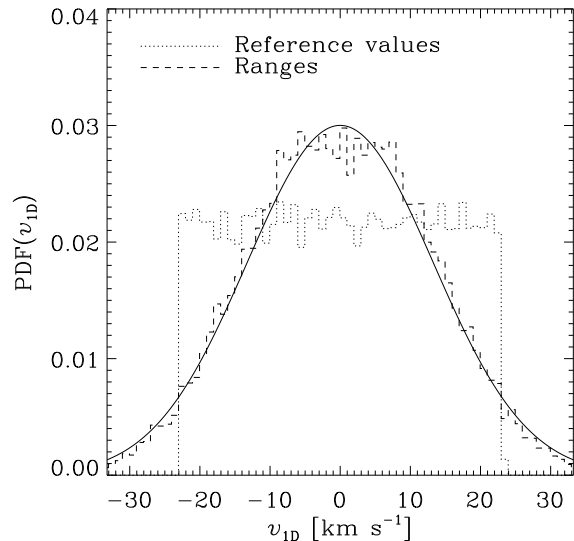


**Figure 1.** Monte Carlo simulations of the probability density functions of  $v_{1\text{D}}$  values of binary populations based on the reference values (i.e. all binaries identical, dotted histogram) and using a spread in the binary parameters (dashed histogram). Both simulations are based on the values for  $m_1$ ,  $q$  and  $\log P$  quoted in Table 2 and both consist of  $10^4$  binaries. The Gaussian curve shown with a full line is the approximation based on the reference values from Table 2, but using  $f = 1$  ( $\sigma_{\text{bin}} = v_{\text{orb}}/\sqrt{3} \approx 13 \text{ km s}^{-1}$ ). This approximation nicely describes the more realistic simulation based on a range of values (dashed histogram).

are acquired by multiplying  $v_{\text{orb}}$  for each binary by a random number between  $-1$  and  $+1$  (Section 2.2). The resulting distribution and the Gaussian approximation ( $\sigma_{\text{bin}} = v_{\text{orb}}/\sqrt{3}$ , Section 2.2) are shown as a dotted histogram and a full line, respectively, in Fig. 1. For the second population we randomly draw values for the masses, mass ratios and periods from the distributions described in Table 2. The binaries with  $P < P_{\text{crit}}$  are taken out of the sample. With equation (3) we then calculate  $v_{\text{orb}}$  for each remaining binary and  $v_{1\text{D}}$  is again acquired by multiplying  $v_{\text{orb}}$  by a random number between  $-1$  and  $+1$ . The resulting distribution is shown as a dashed histogram in Fig. 1. Two things can be seen from this figure: 1.) the width of the more realistic distribution (i.e. using a range in binary parameters) is well approximated by our simple model and 2.) this distribution is close to Gaussian. This last point is important since we have assumed in Section 2.2 that we can quadratically add  $\sigma_{\text{bin}}$  to  $\sigma_{\text{dyn}}$  to get the total velocity dispersion.

#### 2.3.2 The expected dispersion in the binary dispersion

Here we quantify the spread in  $\sigma_{\text{bin}}^2$ , i.e. the dispersion in the additional velocity dispersion squared, when comparing different realisations of binary populations, caused by the fact that the number of binaries is small and that there is a spread in the binary fraction (Table 2).

We generate 1000 massive star populations, each consisting of 200 SGs (an approximate number for a cluster of mass  $10^5 M_\odot$ , Larsen et al. 2008). For each population, we randomly sample a value for  $f$  and thus have  $200 \times f$  binaries. The  $v_{1\text{D}}$  values of the binaries are calculated in the same way as in Section 2.3.1 using the ranges from Table 2. For each population the variance of the 1-

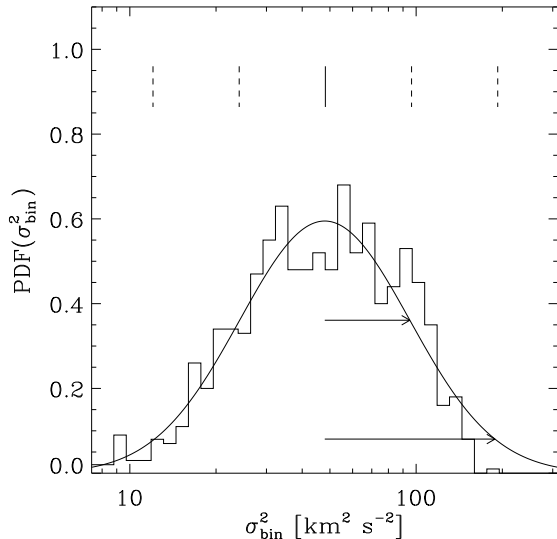


**Figure 2.** The probability density function of  $\sigma_{\text{bin}}^2$  values following from the Monte Carlo experiment described in Section 2.3 for the adopted distributions in  $f$ ,  $m_1$ ,  $q$  and  $\log P$  (Table 2). The solid line near the peak of the distribution indicates the value of  $\sigma_{\text{bin}}^2$  derived with equation (4) using the reference values from Table 2. The dashed lines indicate factors of two of variation. This corresponds approximately to the one and two standard deviations (horizontal arrows) of the log-normal approximation.

dimensional velocity distribution ( $\sigma_{\text{bin}}^2$ ) of the remaining SGs in the sample (single and binary) is then calculated. The resulting probability density function (PDF) of the  $\sigma_{\text{bin}}^2$  values is shown in Fig. 2. The reference value of  $\sigma_{\text{bin}}^2$  is indicated with a vertical solid line and is very close to the mode of the distribution. When approximating PDF( $\sigma_{\text{bin}}^2$ ) by a log-normal we find a standard deviation of  $\sim 0.7$  corresponding to a factor of  $\sim 2$  relative to the mode.

We will now compare the model to empirical determinations of  $M_{\text{dyn}}^{\text{obs}}/M$ . Since we do not know the real mass  $M$  we use  $M_{\text{phot}}$  as a proxy.

### 3 COMPARISON WITH OBSERVATIONS

We illustrate the effect of the presence of binaries by comparing the results of our model from the previous section to the empirical ratio  $M_{\text{dyn}}^{\text{obs}}/M_{\text{phot}}$  for a number of clusters. The cluster masses  $M_{\text{dyn}}^{\text{obs}}$  and  $M_{\text{phot}}$  follow from literature values for magnitude, age,  $\sigma_{\text{obs}}$  and  $r_{\text{eff}}$ . We subsequently re-derive  $M_{\text{phot}}$  and  $M_{\text{dyn}}^{\text{obs}}$  to obtain a homogeneous sample, which is important because the literature values are derived by a number of groups using a variety of SSP models to derive  $M_{\text{phot}}$  and apply different (small) corrections to the value of  $\eta$  (equation 1) because of mass segregation (Fleck et al. 2006) and variations in the density profiles (for those clusters for which measurements of their surface brightness profile are available). All cluster parameters and references to the relevant literature are given in Table 3.

We use the Bruzual & Charlot (2003) SSP models with a Chabrier IMF and solar metallicity to derive  $M_{\text{phot}}$ . For each cluster the age dependent  $M/L$  is found from the observed cluster age. Combining  $M/L$  with the absolute magnitudes ( $M_V$  for 7 clusters, and  $M_K$  for the rest) we determine  $M_{\text{phot}}$ . The quoted upper and lower limits in  $M_{\text{phot}}$  are calculated through the uncertain-

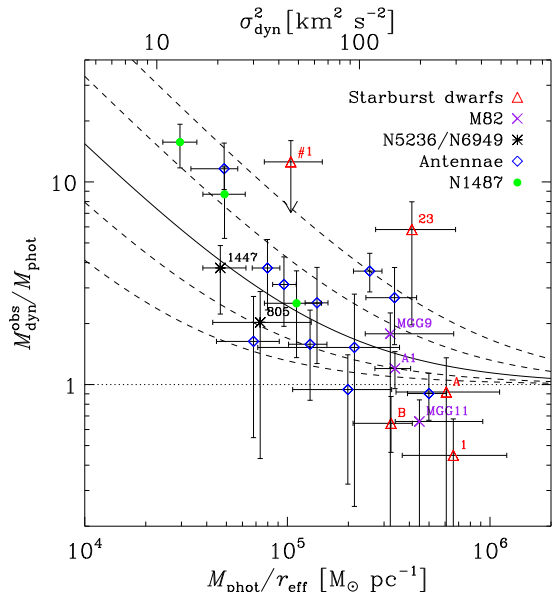


**Figure 3.** The ratio  $M_{\text{dyn}}^{\text{obs}}/M$  as a function of the square of the velocity dispersion expressed in terms of the observables  $M_{\text{phot}}/r_{\text{eff}}$  (equation 1). The solid curve is calculated assuming the fixed binary parameters adopted in Section 2.1, which are:  $f_{\text{SG}} = 0.25$ ,  $q = 0.6$ ,  $m_1 = 15 M_{\odot}$  and  $P = 1000$  days. The dotted curves are calculated by varying  $\sigma_{\text{bin}}^2$  with factors of two for each subsequent curve. The symbols with error bars are the observed values for these parameters from Table 3. The horizontal line is plotted to guide the eye.

ties in  $\log(\text{age}/\text{yr})$ . We use equation (1) to determine  $M_{\text{dyn}}^{\text{obs}}$ , with  $\eta = 9.75$ , and the uncertainty is calculated using the uncertainties in  $\sigma_{\text{obs}}$  and  $r_{\text{eff}}$  by adopting standard error propagation. The calculated values for  $M_{\text{phot}}$  and  $M_{\text{dyn}}^{\text{obs}}$  are presented in Table 3.

We now assume that our choice for the IMF and the metallicity is representative for all clusters and that variations in  $\eta$  due to mass segregation and the density profile are negligible. Under these assumptions  $M_{\text{phot}}$  reflects the true mass  $M$  and subsequently  $\sigma_{\text{dyn}}^2$  scales with  $M_{\text{phot}}/r_{\text{eff}}$  (equation 1). However,  $M_{\text{phot}}$  is also affected by binarity since the shortened RSG phase in short period binaries reduces the integrated luminosity (recently noted by Davies et al. 2009). This effect reduces the fraction of bright stars visible at 10 Myr by a factor of  $(1-g)f \approx 0.5$  (Section 2.1).

In Fig. 3 we present the data. The trend that clusters with a small  $M_{\text{phot}}/r_{\text{eff}}$  tend to have high  $M_{\text{dyn}}^{\text{obs}}/M_{\text{phot}}$ , and which drops with increasing  $M_{\text{phot}}/r_{\text{eff}}$  is well reproduced by a population of binaries among the most massive stars. The dispersion in the observations around the mean value for our model (equation [7], solid curve in Fig. 3) roughly corresponds to the spread following from our Monte Carlo experiment (dashed lines) when allowing a spread in the binary parameters, rather than fixed values.

The linear Pearson correlation coefficient (Rodgers & Nicewander 1988) for the logarithmic values of the data presented in Fig. 3 is  $s = -0.71$  with a significance level (s.l.) of  $\sim 2 \times 10^{-4}$ , which indicates that the observed trend is statistically significant<sup>3</sup>. The downward trend in Fig. 3 suggest that

<sup>3</sup> The coefficient  $s$  can have a value between  $-1$  and  $+1$ , where  $-1(+1)$  indicates a linear relation between the observed variables with negative(positive) slope. A value of  $s = 0$  indicates a lack of correlation.

**Table 3.** Overview of the observational data used. Values for the absolute magnitudes,  $\log(\text{age}/\text{yr})$ ,  $\sigma_{\text{obs}}$  and  $r_{\text{eff}}$  were taken from (1) Östlin et al. (2007); (2) Moll et al. (2007); (3) Larsen et al. (2008); (4) Smith et al. (2006); (5) McCrady & Graham (2007); (6) Bastian et al. (2006, B06) and references therein; (7) McCrady et al. (2003); (8) Mengel et al. (2008, M08). The  $M_V$  value of NGC 6946-1447 was taken from the update given by Larsen et al. (2006). The values for  $M_{\text{dyn}}^{\text{obs}}$  and  $M_{\text{phot}}$  were re-derived in this study, see Section 3 for details.

Galaxy	ID	Ref	$M_V$	$M_K$	$\log(\text{age}/\text{yr})$	$\sigma_{\text{obs}}$ [km s <sup>-1</sup> ]	$r_{\text{eff}}$ [pc]	$M_{\text{dyn}}^{\text{obs}}$ [M <sub>⊙</sub> ]	$M_{\text{phot}}$ [M <sub>⊙</sub> ]	$M_{\text{dyn}}^{\text{obs}}/M_{\text{phot}}$	$M_{\text{phot}}/r_{\text{eff}}$ [10 <sup>5</sup> M <sub>⊙</sub> pc <sup>-1</sup> ]
ESO338-IG	23	1	-15.50		6.85±0.09	32.5±2.5	5.2±1.0	(1.2±0.3) 10 <sup>7</sup>	(2.1 <sup>+1.3</sup> <sub>-0.6</sub> ) 10 <sup>6</sup>	5.8 <sup>+2.2</sup> <sub>-3.9</sub>	4.1 <sup>+2.6</sup> <sub>-1.4</sub>
NGC1140	#1	2	-14.80		6.70±0.15	24.0±1.0	8.0±2.0	(1.0±0.3) 10 <sup>7</sup>	(8.3 <sup>+2.9</sup> <sub>-0.6</sub> ) 10 <sup>5</sup>	12.6 <sup>+0.4</sup> <sub>-5.5</sub>	1.0 <sup>+0.4</sup> <sub>-0.3</sub>
NGC1569	B	3	-12.85		7.30±0.10	9.6±0.3	2.1±0.5	(4.4±1.1) 10 <sup>5</sup>	(6.8 <sup>+0.9</sup> <sub>-1.8</sub> ) 10 <sup>5</sup>	0.6 <sup>+0.2</sup> <sub>-0.2</sub>	3.2 <sup>+0.9</sup> <sub>-1.1</sub>
M82	A1	4,5	-14.84		6.81±0.03	13.4±0.4	3.0±0.5	(1.2±0.2) 10 <sup>6</sup>	(1.0 <sup>+0.1</sup> <sub>-0.1</sub> ) 10 <sup>6</sup>	1.2 <sup>+0.3</sup> <sub>-0.2</sub>	3.4 <sup>+0.7</sup> <sub>-0.7</sub>
M82	MGG9	6,7		-16.23	6.90±0.15	15.9±0.8	2.6±0.4	(1.5±0.3) 10 <sup>6</sup>	(8.4 <sup>+8.7</sup> <sub>-5.6</sub> ) 10 <sup>5</sup>	1.8 <sup>+0.5</sup> <sub>-0.8</sub>	3.2 <sup>+3.4</sup> <sub>-0.8</sub>
M82	MGG11	6,7		-15.75	6.90±0.15	11.4±0.8	1.2±0.2	(3.5±0.7) 10 <sup>5</sup>	(5.4 <sup>+3.6</sup> <sub>-1.0</sub> ) 10 <sup>5</sup>	0.7 <sup>+0.2</sup> <sub>-0.7</sub>	4.5 <sup>+4.7</sup> <sub>-1.1</sub>
NGC1569	A	6	-14.10		7.08±0.20	15.7±1.5	1.9±0.2	(1.1±0.2) 10 <sup>6</sup>	(1.2 <sup>+1.0</sup> <sub>-0.5</sub> ) 10 <sup>6</sup>	0.9 <sup>+0.4</sup> <sub>-0.8</sub>	6.1 <sup>+5.1</sup> <sub>-2.6</sub>
NGC1705	1	6	-14.00		7.08±0.20	11.4±1.5	1.6±0.2	(4.7±1.4) 10 <sup>5</sup>	(1.1 <sup>+0.9</sup> <sub>-0.4</sub> ) 10 <sup>6</sup>	0.4 <sup>+0.2</sup> <sub>-0.2</sub>	6.6 <sup>+5.5</sup> <sub>-2.9</sub>
NGC5236	805	6	-12.17		7.10±0.20	8.1±0.2	2.8±0.4	(4.2±0.6) 10 <sup>5</sup>	(2.1 <sup>+1.6</sup> <sub>-0.8</sub> ) 10 <sup>5</sup>	2.0 <sup>+0.9</sup> <sub>-1.6</sub>	0.7 <sup>+0.6</sup> <sub>-0.3</sub>
NGC6946	1447	6	-13.19		7.05±0.10	8.8±1.0	10.2±1.6	(1.8±0.5) 10 <sup>6</sup>	(4.8 <sup>+1.4</sup> <sub>-0.5</sub> ) 10 <sup>5</sup>	3.8 <sup>+1.1</sup> <sub>-1.5</sub>	0.5 <sup>+0.2</sup> <sub>-0.1</sub>
NGC4038	W99-1	6	-14.00		6.91±0.20	9.1±0.6	3.6±0.5	(6.8±1.3) 10 <sup>5</sup>	(7.2 <sup>+4.5</sup> <sub>-3.2</sub> ) 10 <sup>5</sup>	0.9 <sup>+0.5</sup> <sub>-0.6</sub>	2.0 <sup>+1.3</sup> <sub>-0.9</sub>
NGC4038	W99-16	6	-12.70		7.00±0.10	15.8±1.0	6.0±0.5	(3.4±0.5) 10 <sup>6</sup>	(2.9 <sup>+0.4</sup> <sub>-0.9</sub> ) 10 <sup>5</sup>	11.6 <sup>+3.9</sup> <sub>-2.4</sub>	0.5 <sup>+0.1</sup> <sub>-0.2</sub>
NGC4038	W99-2	8		-17.40	6.82±0.02	14.1±1.0	8.0±1.5	(3.6±0.8) 10 <sup>6</sup>	(4.0 <sup>+0.5</sup> <sub>-0.4</sub> ) 10 <sup>6</sup>	0.9 <sup>+0.2</sup> <sub>-0.2</sub>	5.0 <sup>+1.1</sup> <sub>-1.1</sub>
NGC4038	W99-15	8		-15.50	6.94±0.01	20.2±1.5	1.4±0.2	(1.3±0.3) 10 <sup>6</sup>	(3.6 <sup>+0.2</sup> <sub>-0.3</sub> ) 10 <sup>5</sup>	3.6 <sup>+0.8</sup> <sub>-0.8</sub>	2.5 <sup>+0.4</sup> <sub>-0.4</sub>
NGC4038	S1_1	8		-15.70	6.90±0.02	12.5±3.0	3.6±0.3	(1.3±0.6) 10 <sup>6</sup>	(5.0 <sup>+0.5</sup> <sub>-0.5</sub> ) 10 <sup>5</sup>	2.5 <sup>+1.3</sup> <sub>-1.3</sub>	1.4 <sup>+0.2</sup> <sub>-0.2</sub>
NGC4038	S1_2	8		-15.40	6.92±0.02	11.5±2.0	3.6±0.4	(1.1±0.4) 10 <sup>6</sup>	(3.5 <sup>+0.3</sup> <sub>-0.2</sub> ) 10 <sup>5</sup>	3.1 <sup>+1.1</sup> <sub>-1.2</sub>	1.0 <sup>+0.1</sup> <sub>-0.1</sub>
NGC4038	S1_5	8		-14.80	6.93±0.02	12.0±3.0	0.9±0.6	(2.9±2.4) 10 <sup>5</sup>	(1.9 <sup>+0.1</sup> <sub>-0.1</sub> ) 10 <sup>5</sup>	1.5 <sup>+1.3</sup> <sub>-1.3</sub>	2.1 <sup>+1.4</sup> <sub>-1.4</sub>
NGC4038	2000_1	8		-16.80	6.93±0.02	20.0±3.0	3.6±1.0	(3.3±1.3) 10 <sup>6</sup>	(1.2 <sup>+0.1</sup> <sub>-0.0</sub> ) 10 <sup>6</sup>	2.7 <sup>+1.3</sup> <sub>-1.1</sub>	3.4 <sup>+1.0</sup> <sub>-0.9</sub>
NGC4038	S2_1	8		-15.20	6.95±0.01	11.5±2.0	3.7±0.5	(1.1±0.4) 10 <sup>6</sup>	(3.0 <sup>+0.2</sup> <sub>-0.2</sub> ) 10 <sup>5</sup>	3.8 <sup>+1.4</sup> <sub>-1.4</sub>	0.8 <sup>+0.1</sup> <sub>-0.1</sub>
NGC4038	S2_2	8		-15.30	6.95±0.01	9.5±2.0	2.5±0.5	(5.1±2.4) 10 <sup>5</sup>	(3.2 <sup>+0.2</sup> <sub>-0.3</sub> ) 10 <sup>5</sup>	1.6 <sup>+0.7</sup> <sub>-0.7</sub>	1.3 <sup>+0.3</sup> <sub>-0.3</sub>
NGC4038	S2_3	8		-14.80	6.95±0.01	7.0±2.0	3.0±1.0	(3.3±2.2) 10 <sup>5</sup>	(2.0 <sup>+0.1</sup> <sub>-0.2</sub> ) 10 <sup>5</sup>	1.6 <sup>+1.1</sup> <sub>-1.1</sub>	0.7 <sup>+0.2</sup> <sub>-0.2</sub>
NGC1487	1	8		-14.20	6.92±0.03	13.7±2.0	2.3±0.5	(9.8±3.6) 10 <sup>5</sup>	(1.1 <sup>+0.2</sup> <sub>-0.0</sub> ) 10 <sup>5</sup>	8.7 <sup>+3.2</sup> <sub>-3.4</sub>	0.5 <sup>+0.1</sup> <sub>-0.1</sub>
NGC1487	2	8		-14.20	6.93±0.02	11.1±1.8	1.0±0.3	(2.8±1.2) 10 <sup>5</sup>	(1.1 <sup>+0.1</sup> <sub>-0.1</sub> ) 10 <sup>5</sup>	2.5 <sup>+1.1</sup> <sub>-1.2</sub>	1.1 <sup>+0.4</sup> <sub>-0.3</sub>
NGC1487	3	8		-13.40	6.93±0.02	14.3±1.0	1.8±0.3	(8.3±1.8) 10 <sup>5</sup>	(5.3 <sup>+0.7</sup> <sub>-0.3</sub> ) 10 <sup>4</sup>	15.7 <sup>+3.5</sup> <sub>-4.0</sub>	0.3 <sup>+0.1</sup> <sub>-0.1</sub>

$\sigma_{\text{obs}}^2$  equals  $\sigma_{\text{dyn}}^2$  plus a constant. This is what follows if all clusters are virialised and host a similar binary population (equation 6).

#### 4 CONCLUSIONS AND DISCUSSION

Several studies have found from spectroscopic analyses that for many young ( $\sim 10$  Myr) star clusters the measured velocity dispersion is too high for the mass derived from their total luminosities and their ages. This has led several authors to conclude that these clusters are super-virial and thus dissolving. However, the conversion from velocity dispersion to mass (equation 1) does not consider the additional velocities of binaries. K08 considered this effect, but concluded that binaries are only important for clusters with low intrinsic velocity dispersion ( $\sim 1$  km s<sup>-1</sup>), i.e. lower than the aforementioned clusters. K08 ignored the mass dependent mass-to-light ratio of stars and the intrinsically different binary properties of massive stars. In this study we show that taking these aspects into account makes the contribution of binarity to the dynamical mass estimates,  $M_{\text{dyn}}^{\text{obs}}$ , of clusters in this age range non-negligible.

We present a simple analytical model that gives the 1-dimensional velocity dispersion of a virialised star cluster hosting a binary population. The model is complementary to the classical virial relation for clusters consisting of single stars (equation 1). The result is presented as a single equation that needs as input the (typical) binary fraction, mass ratio, primary mass and orbital period of the binary population and the mass and radius of the star cluster. This relation can be used to easily estimate the effect of binaries based on different parameters for the binary population and/or cluster. The model presented here serves as a starting point for more realistic approaches using binary population synthesis

models (e.g. Eldridge & Stanway 2009). Tentative confirmation of our results comes from the velocity dispersion of the binary population discussed in E08:  $\sim 12$  km s<sup>-1</sup> at an age of 10 Myr (Eldridge 2009, priv. comm.), which is close to what we find for the reference values discussed in Section 2 (see Fig. 1).

For 24 clusters we derive the ratio of  $M_{\text{dyn}}^{\text{obs}}$  over the photometric mass,  $M_{\text{phot}}$ , and show that it decreases with increasing cluster velocity dispersion. This is also what follows from the model and most of the empirically determined  $M_{\text{dyn}}^{\text{obs}}/M_{\text{phot}}$  ratios can be explained by binaries using a conservative binary fraction of 25%, a mass ratio of 0.6 and an orbital period of a 1000 days. When allowing a spread in the binary parameters, almost all clusters are within 2-standard deviation of the model results.

The fact that  $M_{\text{dyn}}^{\text{obs}}$  and  $M_{\text{phot}}$  generally agree for older ( $\gtrsim 100$  Myr) clusters is consistent with this binary scenario. In older clusters, we indeed expect a lower velocity contribution of binaries. The primary star will be of a later spectral type, thus  $m_1$  is lower. At 100 Myr the most luminous stars are roughly  $5 M_{\odot}$ . Equation (4) shows that when  $m_1$  is a factor of 3 lower,  $\sigma_{\text{bin}}^2$  is a factor of  $\sim 2$  lower, keeping all other parameters fixed. Also, typical periods are longer. Duquennoy & Mayor (1991) find that the median period of solar type stars is 180 yr. From equation (4) we can see that the effect of such binaries on  $\sigma_{\text{bin}}^2$  is about a factor of  $\sim 15$  less than the (early type) binaries considered here.

As mentioned in Section 3, the estimated  $M_{\text{phot}}$  following from a comparison with SSP models, or from an IMF extrapolation from the number of RSGs as is done in resolved clusters, is also affected by binarity (Davies et al. 2009). The fraction of stars that is removed from our sample due to this effect is  $(1-g)f$ , corresponding to 45%, giving rise to  $M_{\text{dyn}}^{\text{obs}}/M_{\text{phot}} \approx 2$  for the values of Table 2. There is no reason, however, to expect that this would

preferentially affect clusters with low ratios  $M_{\text{phot}}/r_{\text{eff}}$  and it can thus not cause the downward trend seen in Fig. 3.

The values of the binary parameters used in the study (Table 2) are only indirectly based on observations since we have to correct the period distribution found for massive main-sequence stars to account for the reduced RSG phase of stars in tight binaries (section 2.1). Our assumption can be verified once the binary fraction  $f_{\text{SG}}$  and the associated period distribution among a statistically significant sample of resolved SGs has been determined. This could be done spectroscopically using a long time base ( $\sim$ few 100 – 1000 d). The recently discovered RSG clusters towards the Galactic centre (Figer et al. 2006; Davies et al. 2007; Clark et al. 2009) provide an excellent opportunity to do this. All three have approximately the same age as the extra-galactic clusters used here and their masses are relatively low (few times  $10^4 M_{\odot}$ ) and have radii of a few pc, which according to our model places them in the regime where binaries dominate the measured velocity dispersion. The ratio  $M_{\text{dyn}}^{\text{obs}}/M_{\text{phot}}$  was determined for two of them and is  $\sim 2$  (Davies et al. 2008), lower than the extra-galactic clusters with comparable  $M_{\text{phot}}/r_{\text{eff}}$  (Fig. 3), but still consistent with the lower  $2\sigma$  line of our prediction. This result is very sensitive to low number statistics since the number of RSG in these clusters is  $\sim 20$ , so for  $f_{\text{SG}} = 0.25$  we expect only a handful of binaries.

Ritchie et al. (2009) present a spectroscopic multi-epoch survey of luminous evolved stars in Westerlund 1. This cluster is slightly younger than the clusters considered here, thus its supergiants population is formed by more massive stars. They find a binary fraction in excess of 40% among the 20 most luminous supergiants. Interestingly, they also find radial velocity changes of  $\sim 15 - 25 \text{ km s}^{-1}$  in cool hypergiants due to photospheric pulsations. Macro turbulence dispersions of  $5 - 10 \text{ km s}^{-1}$  are also found for luminosity class II and III giants by Gray & Toner (1986) and Carney et al. (2008). This is an additional complication in dynamical mass determinations of young star clusters containing massive giants.

Our results are an important ingredient in the discussion on the importance of the early mass independent disruption, or ‘infant mortality’, of star clusters. The high velocity dispersions found for the clusters discussed here have been put forward as empirical evidence that many young ( $\lesssim 30 \text{ Myr}$ ) clusters are quickly dissolving (e.g. Goodwin & Bastian 2006, M08). We have provided arguments that the alleged super-virial state can largely be explained by orbital motions of binary stars.

Early dissolution due to gas expulsion can still exist, but it probably occurs on much shorter time-scales ( $\ll 10 \text{ Myr}$ ) than generally assumed. This idea is supported by the fact that the clusters considered here have densities of  $\sim 10^3 M_{\odot} \text{ pc}^{-3}$ , corresponding to an internal crossing times of the stars of roughly  $0.5 \text{ Myr}$ . So these clusters have evolved for at least 20 crossing times. The crossing time in the embedded phase is much shorter than the crossing time at  $10 \text{ Myr}$  due to the nonzero star formation efficiency and the consequent expansion (Bastian et al. 2008). The gas expulsion models show that clusters need about 20 initial crossing times to find a new virial equilibrium, or completely dissolve into the field (e.g. Goodwin 1997; Geyer & Burkert 2001; Baumgardt & Kroupa 2007). So at  $10 \text{ Myr}$  the super-virial state is undetectable and the clusters discussed here are therefore survivors of the gas expulsion, or ‘infant mortality’, phase.

## ACKNOWLEDGEMENT

The authors thank John Eldridge and Selma de Mink for helpful discussions on the evolutionary path of massive binaries and the referee, Ben Davies, for helpful suggestions. This work was supported by NWO grant # 639.073.803.

## REFERENCES

- Bastian N., Gieles M., Goodwin S. P., Tranco G., Smith L. J., Konstantopoulos I., Efremov Y., 2008, MNRAS, 389, 223  
 Bastian N., Saglia R. P., Goudfrooij P., Kissler-Patig M., Maraston C., Schweizer F., Zoccali M., 2006, A&A, 448, 881 (B06)  
 Baumgardt H., Kroupa P., 2007, MNRAS, 380, 1589  
 Bosch G., Terlevich E., Terlevich R., 2009, AJ, 137, 3437  
 Bruzual G., Charlot S., 2003, MNRAS, 344, 1000  
 Carney B. W., Gray D. F., Yong D., Latham D. W., Manset N., Zelman R., Laird J. B., 2008, AJ, 135, 892  
 Clark J. S., Negueruela I., Davies B., Larionov V. M., Ritchie B. W., Figer D. F., Messineo M., Crowther P. A., Arkharov A. A., 2009, A&A, 498, 109  
 Davies B., Figer D. F., Kudritzki R.-P., MacKenty J., Najarro F., Herrero A., 2007, ApJ, 671, 781  
 Davies B., Figer D. F., Law C. J., Kudritzki R., Najarro F., Herrero A., MacKenty J. W., 2008, ApJ, 676, 1016  
 Davies B., Origlia L., Kudritzki R.-P., Figer D. F., Rich R. M., Najarro F., Negueruela I., Clark J. S., 2009, ApJ, 696, 2014  
 Duquennoy A., Mayor M., 1991, A&A, 248, 485  
 Eggleton P. P., 1983, ApJ, 268, 368  
 Eldridge J. J., Izzard R. G., Tout C. A., 2008, MNRAS, 384, 1109 (E08)  
 Eldridge J. J., Stanway E. R., 2009, arXiv:0908.1386  
 Figer D. F., MacKenty J. W., Robberto M., Smith K., Najarro F., Kudritzki R. P., Herrero A., 2006, ApJ, 643, 1166  
 Fleck J.-J., Boily C. M., Lançon A., Deiters S., 2006, MNRAS, 369, 1392  
 Gaburov E., Gieles M., 2008, MNRAS, 391, 190  
 Geyer M. P., Burkert A., 2001, MNRAS, 323, 988  
 Goodwin S. P., 1997, MNRAS, 286, 669  
 Goodwin S. P., Bastian N., 2006, MNRAS, 373, 752  
 Gray D. F., Toner C. G., 1986, ApJ, 310, 277  
 Hills J. G., 1980, ApJ, 235, 986  
 Kouwenhoven M. B. N., de Grijs R., 2008, A&A, 480, 103 (K08)  
 Lada C. J., Lada E. A., 2003, ARA&A, 41, 57  
 Larsen S. S., 2004, A&A, 416, 537  
 Larsen S. S., Brodie J. P., Hunter D. A., 2004, AJ, 128, 2295  
 Larsen S. S., Brodie J. P., Hunter D. A., 2006, AJ, 131, 2362  
 Larsen S. S., Origlia L., Brodie J., Gallagher J. S., 2008, MNRAS, 383, 263  
 Lejeune T., Schaerer D., 2001, A&A, 366, 538  
 Mason B. D., Hartkopf W. I., Gies D. R., Henry T. J., Helsel J. W., 2009, AJ, 137, 3358  
 McCrady N., Gilbert A. M., Graham J. R., 2003, ApJ, 596, 240  
 McCrady N., Graham J. R., 2007, ApJ, 663, 844  
 Mengel S., Lehnert M. D., Thatte N. A., Vacca W. D., Whitmore B., Chandar R., 2008, A&A, 489, 1091 (M08)  
 Miller B. W., Whitmore B. C., Schweizer F., Fall S. M., 1997, AJ, 114, 2381  
 Moll S. L., Mengel S., de Grijs R., Smith L. J., Crowther P. A., 2007, MNRAS, 382, 1877  
 Östlin G., Cumming R. J., Bergvall N., 2007, A&A, 461, 471

- Portegies Zwart S. F., Pooley D., Lewin W. H. G., 2002, *ApJ*, 574, 762
- Ritchie B. W., Clark J. S., Negueruela I., Crowther P. A., 2009, arXiv:0909.3815
- Rodgers J., Nicwander W., 1988, *The American Statistician*, 42, 59
- Sana H., Gosset E., Evans C. J., 2009, *MNRAS*, in press
- Sana H., Gosset E., Nazé Y., Rauw G., Linder N., 2008, *MNRAS*, 386, 447
- Sana H., Le Bouquin J.-B., 2009, in Rivinius T., ed., *Rev. Mex. Conf. Ser.*, in press (arXiv:0906.5003), The interferometric view of Hot Stars. The place of interferometry in massive star multiplicity studies
- Smith L. J., Westmoquette M. S., Gallagher J. S., O'Connell R. W., Rosario D. J., de Grijs R., 2006, *MNRAS*, 370, 513
- Spitzer L., 1987, *Dynamical evolution of globular clusters*. Princeton, NJ, Princeton University Press, 1987, 191 p.
- Vanbeveren D., De Loore C., Van Rensbergen W., 1998, *A&A Rev.*, 9, 63
- Whitmore B. C., Schweizer F., 1995, *AJ*, 109, 960
- Zepf S. E., Ashman K. M., English J., Freeman K. C., Sharples R. M., 1999, *AJ*, 118, 752